

Article

Can a Simple Static-Equivalent Model Be Used to Predict Major Trends in the Dynamic Structural Response of Monopile Offshore Wind Turbines?

Antonio J. Romero-Monzón , Carlos Romero-Sánchez , Guillermo M. Álamo  and Luis A. Padrón * 

Instituto Universitario de Sistemas Inteligentes y Aplicaciones Numéricas en Ingeniería (SIANI), Universidad de Las Palmas de Gran Canaria (ULPGC), Edificio Central del Parque Científico y Tecnológico, Campus Universitario de Tafira, 34017 Las Palmas de Gran Canaria, Spain; antonio.romero104@alu.ulpgc.es (A.J.R.-M.); carlos.romero@ulpgc.es (C.R.-S.); guillermo.alamo@ulpgc.es (G.M.Á.)

* Correspondence: luis.padron@ulpgc.es

Abstract: This paper tests the capability of a simplified model to predict major trends in the dynamic structural response of monopile offshore wind turbines. For this purpose, the results of two numerical models of different levels of complexity are compared: the advanced time-domain multi-physics tool OpenFAST and a simplified static-equivalent model based on beam elements and concentrated masses. The IEA-15-240-RWT reference wind turbine is considered as a benchmarking problem. The comparison between the two structural models is presented in terms of their fundamental frequencies and through the analysis of shear forces and bending moments under wind-only and combined wave and wind load scenarios. The results show that the simplified model can adequately represent the system's mass and stiffness characteristics, as well as the impact of soil–structure interaction effects on its fundamental frequency. Turbulence and wind velocity have a significant impact on internal forces and on the ability of the simplified model to reproduce their values. Despite the large differences obtained for highly turbulent scenarios, the acceptable accuracy obtained for relevant load scenarios and the conservative nature of the simplified model make it a viable option for preliminary large-scale studies that prioritize efficiency and efficacy over high-precision.

Keywords: offshore wind turbine; soil–structure interaction; monopile foundation; OpenFAST; static-equivalent analysis



Academic Editor: Wei Huang

Received: 19 January 2025

Revised: 31 January 2025

Accepted: 4 February 2025

Published: 6 February 2025

Citation: Romero-Monzón, A.J.; Romero-Sánchez, C.; Álamo, G.M.; Padrón, L.A. Can a Simple Static-Equivalent Model Be Used to Predict Major Trends in the Dynamic Structural Response of Monopile Offshore Wind Turbines? *Appl. Sci.* **2025**, *15*, 1633. <https://doi.org/10.3390/app15031633>

Copyright: © 2025 by the authors. Licensee MDPI, Basel, Switzerland. This article is an open access article distributed under the terms and conditions of the Creative Commons Attribution (CC BY) license (<https://creativecommons.org/licenses/by/4.0/>).

1. Introduction

Over the last few decades, offshore wind energy has experienced significant advancements due to the necessity of alternative energy sources in the transition from fossil fuels to renewable energies. This is motivated by the more favorable conditions offered by the marine environment compared to land. Regarding the current state of offshore wind energy, in 2023, the offshore wind energy sector experienced a significant expansion, marking its second most productive year with the commissioning of 11 GW in new projects. By year's end, the cumulative global capacity soared to 1 TW. Based on the current growth trajectory, projections indicate that the 2 TW threshold could be reached before 2030. The industry's expansion is accelerating, with another annual record shattered in 2024. However, this growth remains heavily concentrated in major markets, including China, the European Union, the United States, India, and Brazil [1].

Nevertheless, to ensure the efficiency of this technology, it is crucial to analyze how structures respond to environmental factors such as wind and waves as it is defined in

several standards and design guidelines [2–4]. This analysis is complex due to the variety of phenomena involved, including aeroelastic effects, fluid–structure or soil–structure interaction (SSI), and the proper modeling of the turbine control system and the uncertainty associated with certain parameters.

Regarding wind turbines, the foundation is a crucial element in their design, as it is responsible for transferring the loads from the wind turbine to the ground and depends on both the specifications of the wind turbine and the load-bearing capacity of the terrain. Moreover, additional challenges are present in the marine environment, such as chloride corrosion or the complexities in their installation. The foundations of offshore wind turbines (OWTs) are divided into two main categories: foundations fixed to the seabed and those with floating supports usually anchored with chains. Out of the 68 258 MW in existing offshore wind energy projects, monopiles are the predominant substructure type (55.6%), followed by jackets (13.4%), pile caps (7.6%), tripods (1.6%), and gravity-base (1.3%) designs [5].

In this particular work, monopile foundations are analyzed. They consist of tubular steel structures used to anchor the towers of the wind turbines to the seabed. Although they can be installed up to 40 m deep, their use is more common in shallower waters, and it is the most widespread type of foundation in the offshore wind industry due to its versatility. Monopiles present advantages such as their simple design or their effectiveness in sandy or clay soils without requiring prior preparation of the terrain. However, their disadvantages include the high costs and risks associated with installation and transport, as well as the need for heavy machinery for their placement, which can negatively affect marine life. In terms of their geometry, monopiles are composed of two distinct parts: the monopile itself and the transition piece.

Simplified procedures are often used to carry out a preliminary analysis of the structure based on the environmental characteristics of the site. One of the most widely used methods is the one developed by Arany et al. [6], where the design of a monopile is defined in ten steps using an iterative calculation procedure and transferring wind and wave loads in a simplified way to the mudline level. Numerous studies have employed simplified procedures in the design of monopiles. For instance, Luo et al. [7] presented a method for laterally loaded rigid monopiles in cohesionless soil, while Burd et al. [8] applied the PISA design model to marine sand. Additionally, the rapid approach for structural design by NREL [9] provides baseline designs for a 25 MW turbine in a simplified way. These studies, among others, highlight the effectiveness of simplified methods in preliminary design stages. Other notable works include the application of the PISA design model to monopiles embedded in layered soils [10].

In contrast, more complex frameworks, such as the one provided by the OpenFAST code, are used for studying aerodynamic, hydrodynamic, elastic, and structural characteristics in wind turbines. OpenFAST has been widely used for the detailed analysis and optimization of monopile designs, as the fact that it is open-source software allows for its continuous evolution. The first study by Jonkman [11] investigates the coupled dynamic response of OWTs using this comprehensive aero-hydro-servo-elastic simulation tool, highlighting the importance of considering the interaction between aerodynamic, hydrodynamic, and structural dynamics. Luan et al. [12] conducted an optimization study of a tuned mass damper for large monopile wind turbines. These studies demonstrate the capabilities of OpenFAST in capturing complex interactions, such as soil–structure interaction effects. Other significant contributions include a study by Jonkman [13] on the dynamic responses of offshore wind turbines using FAST, and research by Barahona et al. [14] comparing FAST results with previous international code-comparison projects. Additionally, the work by

Jonkman [15] on the validation of FAST for OWT applications is also representative of the noteworthy capabilities of this software.

The choice of the structural model depends on the type of problem, its complexity, and the desired level of precision. Different numerical models should not be considered mutually exclusive in their application. In the initial stages of structural design for wind turbines, simplified models are an appropriate tool to begin addressing the problem using minimal computational resources. Their simplified nature also reduces complexity in data processing and requires less time. However, for detailed structural analysis in later stages, time-domain multi-physics tools provide a broader and more detailed approach, allowing for a deeper study of the problem. However, the comparison between a simplified model approach and more rigorous time-domain multi-physics tools (software such as OpenFAST, HAWC2 or Bladed, among others) is crucial to validate the accuracy of these models and evaluate their reliability. In this field, to the authors' knowledge, only Jawalageri et al. [16] have conducted a study comparing OpenFAST with simplified formulas for environmental load combinations described by Arany et al. [6]. They focused on comparing maximum bending moments at the mudline level and shear forces at hub height for extreme environmental conditions.

The objective of this paper is helping to elucidate whether or not a simplified static-equivalent model can be used to predict major trends in the dynamic structural response of monopile OWTs. To do so, this study presents a comparison between the results of two numerical models of different levels of complexity used for estimating the structural response of OWTs under dynamic loads: the advanced time-domain multi-physics numerical tool OpenFAST and a simplified static-equivalent model based on beam elements and lumped masses. The results of this simplified model are compared to those of the baseline OpenFAST model in terms of fundamental frequencies, and shear forces, and bending moments along the system. To achieve this, a series of simulations are conducted, including scenarios with only wind loads and with combined wind and wave loads, corresponding to normal operation and extreme conditions.

The present paper is structured into five sections. After this introduction, Section 2 presents the methodology, detailing the two numerical models used, including soil–structure interaction phenomena. Section 3 describes the properties of the OWT, the environmental conditions adopted in this study, and the complete set of cases analyzed. Section 4 discusses the results obtained from both numerical models. Finally, Section 5 summarizes the main conclusions of this work, in which the ability of the simplified model to reproduce the response of the multi-physics tool is discussed.

2. Methods

Two models are compared to obtain the structural response of the monopile–OWT system: (1) a simplified static-equivalent model based on beam elements and concentrated masses and (2) a multi-physics multi-domain time-dependent model (OpenFAST). In the following sections, the main characteristics and assumptions of each model are outlined.

2.1. Simplified Static-Equivalent Model

The simplified model is based on a discretization of the system's geometry into beam elements, a concentrated mass representing the rotor–nacelle assembly, and the assumption of static-equivalent loads for the environmental excitation arising from wind and wave action. For this particular study, in which wind and wave loads are assumed to be aligned, a two-dimensional approach to simulate the lateral behavior of the structure was considered. A sketch of the simplified model is depicted in Figure 1. The code of the simplified model is included in the Supplementary Materials.

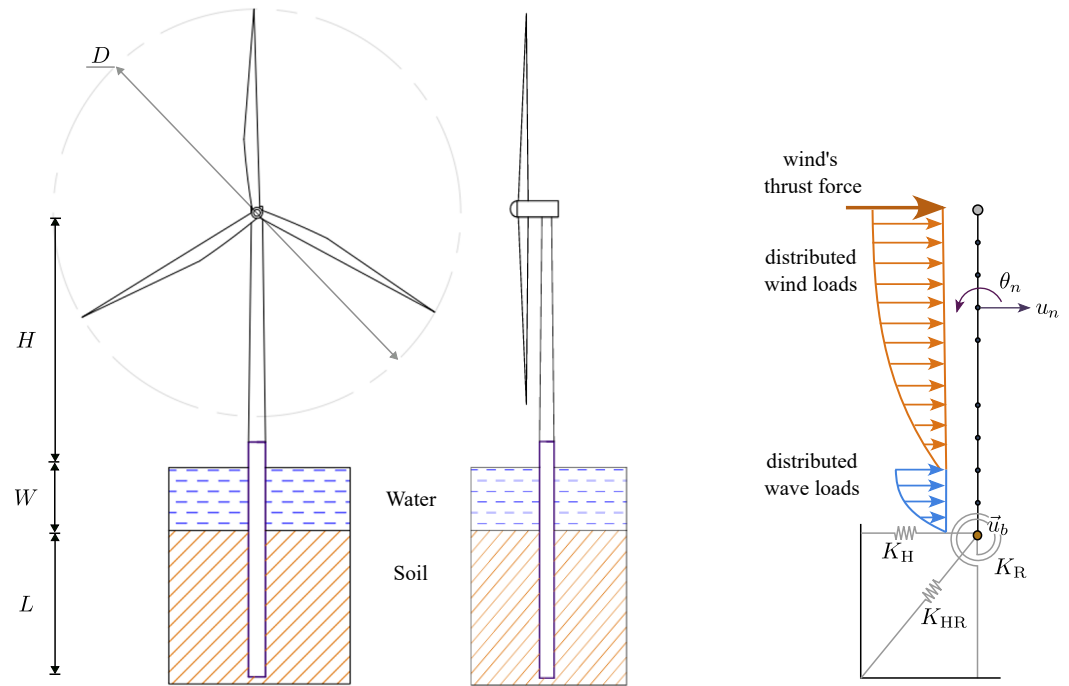


Figure 1. Sketch of the real problem (left) and simplified static-equivalent model (right). Adapted from [17].

The wind turbine’s hollow tower and monopile were divided into two-node Euler–Bernoulli beam elements. Based on a convergence study, a sufficiently large number of elements was used to accurately reproduce the conical shape of the tower. Each node has two degrees of freedom: a lateral displacement (u_n) and a rotation (θ_n), as shown in Figure 1.

The interaction between the structure and the foundation was modeled using the foundation impedance matrix (K_{SSI}), which represents the stiffness of the soil–monopile subsystem. As a static-equivalent analysis was carried out, the static component was considered. As shown in Equation (1), this matrix consists of horizontal (K_H), rocking (K_R), and cross-coupled (K_{RH} and K_{HR}) terms:

$$K_{SSI} = \begin{pmatrix} K_H & K_{HR} \\ K_{RH} & K_R \end{pmatrix} \quad (1)$$

To compute the foundation impedance matrix, a numerical model [18] previously developed for the dynamic analysis of pile foundations was used. This model utilizes the integral expression of the Reciprocity Theorem along with specific Green’s functions for a layered half-space to represent soil behavior. In this formulation, piles are modeled as load lines in terms of soil–pile interaction forces. Additionally, the additional stiffness introduced by the piles is represented using a beam finite element model. Soil and pile variables are coupled by enforcing compatibility and equilibrium conditions at the soil–pile interface in terms of displacements and interaction forces. The main advantage of this model is its ability to accurately reproduce the linear response of the soil–foundation system without discretizing soil variables, resulting in a compact and efficient formulation. The effectiveness of this model in reproducing foundation behavior for OWT monopile and bucket geometries was validated in [19].

In assembling the stiffness matrices of all beam elements, including the additional stiffness introduced by the foundation, the following system was defined in order to obtain the structural static response:

$$\begin{pmatrix} K_{ss} & K_{sb} \\ K_{bs} & K_{bb} + K_{SSI} \end{pmatrix} \begin{Bmatrix} \vec{u}_s \\ \vec{u}_b \end{Bmatrix} = \vec{F}_{ext} \quad (2)$$

where the vector \vec{u}_s refers to the displacements and rotations of the active degrees of freedom of the superstructure, while the vector \vec{u}_b represents the displacement and rotation at its base, i.e., the pile head at the mudline level. Finally, \vec{F}_{ext} denotes the static-equivalent external loads applied to the structure. In the proposed model, only wind and wave loads are considered. Their treatment is outlined in Sections 2.1.2 and 2.1.3, respectively. It is important to notice that, due to the isostatic nature of the model, the internal forces at a specific point of the structure can be obtained directly as the sum of the corresponding forces/moments acting above the studied point.

2.1.1. Dynamic Characterization of the System

Although a static approach was considered to obtain the structural response in terms of stresses, one of the main requirements imposed by recommended practices and guidelines is to avoid structural resonance. For this purpose, the fundamental frequency of the system should avoid matching the rotor and blade-passing frequencies.

In order to estimate the fundamental frequency of the system with the simplified model, distributed inertial properties were assumed for the beam elements, representing the monopile and tower mass. On the other hand, the mass of the rotor–nacelle assembly was considered a concentrated mass at the top node, while no punctual moments of inertia were considered, as their impact on the fundamental frequency of the system was expected to be negligible.

In marine environments, fluid–structure interaction leads accelerated bodies in fluid to experience greater inertia forces due to the added mass of surrounding fluid particles. This added mass, varying with body geometry, can be mathematically considered as a weighted integration of these particles' masses [20]. Also, assuming that the monopile is filled with water, the structural oscillation mobilizes the internal fluid. For simplicity, these two fluid–structure interaction effects were considered as an additional punctual mass at each submerged node with the following value:

$$m_a = A_{\text{int}} L_e \rho_w + C_A A L_e \rho_w \approx 2 A L_e \rho_w \quad (3)$$

where A_{int} and A are the areas of the inner and outer circumferences of the monopile, L_e is the element length, ρ_w is the density of water, and C_A is the added mass coefficient, which, for cylinders in flows, takes a unitary value. Note that as the monopile thickness is significantly smaller than its diameter, the enclosed fluid area was assumed to coincide with the area of the outer circumference.

Once the global mass matrix, M , was obtained through the assembly of the elemental masses plus the punctual masses, the undamped fundamental frequency of the system could be obtained by solving the eigenvalue problem:

$$|K - (2\pi f_n)^2 M| = 0 \quad (4)$$

where K is the global stiffness, including SSI effects, as presented in Equation (2).

2.1.2. Wind Loads

The specific reference standards for calculating the action of the wind are IEC 61400-1:2020 [2] and DNVGL-ST-0126 [3]. The thrust force (F_{Th}) that the wind exerts on the rotor is simplified as a static punctual force acting at its level:

$$F_{Th} = \frac{1}{2} \rho_a A_R C_T (\bar{U} + u)^2 \quad (5)$$

where ρ_a is the air density, A_R is the rotor swept area, C_T is the thrust coefficient, and \bar{U} and u are the mean and turbulent components of wind speed. The latter value was computed by following the turbulence models described in the reference standards [2,3], which are also summarized in [6].

On the other hand, the distributed force acting along the parts of the structure above the mean sea level was calculated as follows [21]:

$$dF_{wind} = \frac{1}{2} \rho_a C_D D_i U(z)^2 \quad (6)$$

where C_D is the drag coefficient (a value of 1.2 is considered in accordance with [22]), D_i is the segment diameter, and $U(z)$ is the mean wind velocity at the corresponding height z from the sea level.

2.1.3. Wave Loads

Wave loads were chosen based on Airy linear wave theory, in which a wave profile is represented by a sine function. Firstly, the horizontal particle velocity, w , and horizontal particle acceleration, \dot{w} , were calculated (see, e.g., [6]). At each instant t , the distributed wave force acting over a submerged element was obtained as the sum of two components: the drag force, dF_D , and the inertia force, dF_I :

$$dF_D(z, t) + dF_I(z, t) = \frac{1}{2} \rho_w D_S C_D |w(z, t)| + C_m \rho_w A_S \dot{w}(z, t) \quad (7)$$

where C_D and C_m are the drag and inertia coefficients, whose values are defined in DNV-RP-C205 [23].

The static-equivalent distributed wave load at each level z is assumed to be the sum of the maximum drag and inertia forces that occur in a wave cycle (as the most unfavorable scenario [6]) multiplied by a Dynamic Amplification Factor (DAF) to include its dynamic nature:

$$dF_{wave}(z) = \left(\max_{t \in [0, T_w]} dF_D(z, t) + \max_{t \in [0, T_w]} dF_I(z, t) \right) \cdot \text{DAF} \quad (8)$$

where T_w is the wave period, and the DAF is defined as

$$\text{DAF} = \frac{1}{\sqrt{(1 - (\frac{f_w}{f_n})^2)^2 + (2 \cdot \zeta \cdot \frac{f_w}{f_n})^2}} \quad (9)$$

where $f_w = 1/T_w$ is the wave frequency and ζ is the system damping ratio. In this study, a global damping ratio equal to 1% is considered as a characteristic value of the material damping of steel. The DAF indicates the increment in the dynamic response of the system with respect to the static one derived from the proximity of the excitation and fundamental frequencies. Note that, in the simplified model, the DAF is applied solely to wave loads because the low-frequency wind loads can be directly assumed to be static.

2.2. Time-Domain Multi-Physics Model

The numerical time-domain tool used in this study is OpenFAST. This is a type of open-source software developed in Fortran 95, used for studying both onshore and offshore wind turbines. It is defined as a numerical model that extends the capabilities of the FAST v8 code, analyzing turbines and wind farms through different modules that define and simulate aerodynamic, hydrodynamic, elastic, and structural characteristics. Being open-source, OpenFAST allows users to access and modify its source code, which facilitates its continuous evolution through modifications and improvements stored on a GitHub repository [24].

All the simulations presented in this study were performed while taking into account the following considerations: The aerodynamic loads on the blades and tower were calculated using the AeroDyn module [25], which accounts for rotor wake and induction, blade airfoil aerodynamics, the tower's influence on the fluid near the blade nodes, and tower drag. The wind input files were generated with the program TurbSim [26] and computed with InflowWind [27]. The structural dynamic responses of the rotor, drive-train, nacelle, and tower were modeled using the ElastoDyn module, with a modal formulation for the blades and tower and a multi-body approach for the drive-train and nacelle [28]. The control and electrical drive dynamics were modeled using the ServoDyn module, simulating the control and electrical subsystems of the wind turbine. Wave loads and fluid–structure interaction phenomena were simulated using the HydroDyn module [29], which can use a potential-flow theory solution, a strip-theory solution, or a combination of both to calculate the hydrodynamic loads on the submerged part of the substructure. The structural dynamic response of the substructure, from the transition piece to the base, was computed using the SubDyn module, starting with a linear-frame, finite-element beam discretization of the structure. A more detailed explanation of each module can be found in the OpenFAST Documentation [24].

The SubDyn module [30] was modified to incorporate dynamic soil–structure interaction effects by adjusting the FEM subroutine and the state-space formulation. The implementation developed is described in [31,32], and the code can be found at https://github.com/mmc-siani-es/openfast_3.0.0_multisupport (accessed on 5 February 2025). It uses a lumped parameter model (LPM) at the mudline level to simulate the dynamic interaction between the foundation and soil. The LPM used in this study was initially proposed and validated by Carbonari et al. [33] and later tested in [34,35]. The LPM configuration, characterized by eccentric elements, allows for the simultaneous modeling and fitting of translational, rotational, and horizontal-rocking coupled impedance functions, while the vertical and torsional impedances are modeled using first-order LPMs because of their lesser influence on the turbine's response [36]. To reduce the discrepancies between the two compared models, the frequency-dependent impedance functions considered to adjust the LPM were obtained from the same numerical model [18] considered for the simplified static-equivalent model.

3. Problem Definition

3.1. Reference Wind Turbine Properties

The reference wind turbine considered in this study is the IEA-15-240-RWT [37]. The key characteristics of the wind turbine, tower, and monopile are summarized in Table 1. The structural components of the tower and monopile are assumed to behave elastically, and their mechanical properties are listed in Table 2. The seabed properties are shown in Table 3. These soil properties correspond to a particular case study on the east coast of the USA, also defined in [37].

Table 1. Key parameters of the IEA-15-240-RWT OWT. Extracted from [37].

Parameter	Value
Turbine class	IEC Class 1B
Rating	15 MW
Cut-in wind speed (U_{in})	3 m/s
Rated wind speed (U_R)	10.59 m/s
Cut-out wind speed (U_{out})	25 m/s
Rotor diameter (D)	240 m
Hub height (H)	150 m
RNA mass	1017 ton
Tower mass	860 ton
Tower top diameter	6.5 m
Tower base diameter	10 m
Tower top thickness	24 mm
Tower base thickness	36.5 mm
Water depth (W)	30 m
Pile diameter (d)	10 m
Pile thickness	55.3 mm
Pile depth (L)	45 m
Transition piece height	15 m
Monopile mass	1318 ton
Monopile aspect ratio (L/d)	4.5

Table 2. Steel material properties.

Parameter	Value
Young's modulus	200 GPa
Shear modulus	79.3 GPa
Density	7850 kg/m ³
Damping ratio	0.01

Table 3. Properties of the soil deposit. Extracted from [37].

Parameter	Value
Soil profile	Single layer
Type of soil	Dense sand or gravel
Poisson's ratio	0.4
Density	2000 kg/m ³
Shear modulus	140 MPa
Shear wave velocity	264.5 m/s
Damping ratio	0.05

3.2. Environmental Conditions

The reference environmental conditions used in this paper were also extracted from IEA-15-240-RWT documentation [37]. Wind speed is defined as a Weibull distribution with a shape factor of 2.12. Sea states are characterized by significant wave heights, the peak spectral wave period, and the wave direction. Wave heights and peak spectral periods are representative of the east coast of the USA for a 30 m water depth site. Extreme Sea States (ESSs) and Extreme Wave Heights (EWHs) are calculated following DNVGL-ST-0437 [4], with four categories, which are defined based on the height and frequency of the waves during certain periods. ESS, 1-year and EWH, 1-year refer to extreme waves within a return period of 1 year, where ESS, 1-year is based on the average significant height and EWH, 1-year is based on the maximum recorded height. ESS, 50-years and EWH, 50-years focus on a 50-year period, where ESS, 50-years is based on the average significant height and

EWH, 50-years is based on the maximum height. Significant wave heights for each return period are defined in [37], and the corresponding extreme wave heights are calculated as follows:

$$H_{\text{EWH},T_R} = \left(\sqrt{\frac{1}{2} \left(\frac{3 \cdot 3600}{T_{\text{wave}}} \right)} + \frac{0.2886}{\sqrt{2 \ln \left(\frac{3 \cdot 3600}{T_{\text{wave}}} \right)}} \right) H_{\text{ESS},T_R} \tag{10}$$

where T_R is the return period considered (1 yr or 50 yr), and T_{wave} is the significant wave period. The values considered in this study are shown in Table 4. The wave direction is considered to be aligned with the wind direction (fore-aft direction) in all cases. Finally, the OWT reference documentation does not provide information about current data for the site. Due to this lack of data, the current loads are not considered in this study.

Table 4. Wave data under extreme conditions.

Return Period	Sea State	Wave Height (m)	Peak Spectral Period (s)
1 year	ESS, 1-year	9.686	16.654
	EWB, 1-year	18.204	15.121
50 years	ESS, 50-years	11.307	18.505
	EWB, 50-years	21.092	16.276

3.3. Definition of Study Cases

The comparison of the dynamic responses obtained from the two models considered in this study was conducted for three sets of load cases: (1) parked conditions to obtain the fundamental frequency of the systems, (2) load cases considering just the wind load, and (3) load cases that combine both the wind and wave loads. All OpenFAST simulations were performed over a duration of 400 s with a time step of 0.001 s. For each simulated case, except in the case used to compute the fundamental frequency, the initial 100 s of simulation time were disregarded to ensure that the results were representative of the steady state.

Fundamental frequencies are first analyzed to ensure that the structural models are comparable. The influence of SSI effects in both models is studied by obtaining the fundamental frequencies under fixed-base and flexible-base assumptions. In the time-domain multi-physics simulation of the system with OpenFAST, simulations are conducted around the static equilibrium of the system, considering only gravitational acceleration. In the simplified model, as mentioned before, the fundamental frequencies are obtained by solving the eigenvalue problem.

The second set of load cases focuses on the influence of aeroelastic effects on the response of each model. For this purpose, wind-only load cases are defined using three different types of turbulence: the Normal Turbulence Model (NTM), Extreme Turbulence Model (ETM), and Extreme Operating Gust (EOG). Each type of turbulence is described in IEC 61400-1:2020 [2]. Load scenarios are defined for mean wind speeds ranging from 5 to 25 m/s in increments of 5 m/s, resulting in fifteen scenarios for wind-only loads. The turbulent winds are characterized by the IEC Kaimal wind spectrum and a wind power law exponent. Table 5 summarizes the wind-only scenarios. The EOG turbulence in OpenFAST is simulated using the IEC [2] methodology, which defines this turbulence as a combination of NTM turbulence and a disconnection of the wind turbine from the power grid.

Finally, from the numerous design load combinations defined by the applicable standards and recommendations, four of the five most representative or unfavorable combinations, as described in [6], are considered. These combinations are referred to as environmental load scenarios. The first scenario, E-1, describes the normal operating conditions of the wind turbine, with wind at nominal speed and 1-year extreme wave conditions.

Scenario E-2 addresses an extreme wave scenario with a 50-year return period and wind at nominal speed and extreme turbulence. Scenario E-3 focuses on extreme wind loads, with extreme operational turbulence for a 50-year return period and extreme waves with a 1-year return period. Scenario E-4 considers the cut-out wind speed and extreme operational turbulence with extreme wave conditions, both for a 50-year return period. In all these considered scenarios, the wind and wave loads are assumed to be aligned. A summary of the environmental load scenarios is presented in Table 6.

Table 5. Wind-only scenarios.

Parameter	Values
Turbulence models	NTM, ETM, and EOG
Wind velocities	5, 10, 15, 20, and 25 m/s
Wind spectra	IEC Kaimal spectrum
Wind shear	Power law exponent

Table 6. Environmental load scenarios extracted from Arany et al. [6].

Scenario	Wind Conditions	Wave Conditions
E-1	NTM at U_R	ESS-1 yr
E-2	ETM at U_R	EWH-50 yr
E-3	EOG at U_R	EWH-1 yr
E-4	EOG at U_{out}	EWH-50 yr

4. Results

In the following sections, the results corresponding to the three sets of load scenarios defined in Section 3.3 are presented. The structural responses obtained with the simplified static-equivalent model and the time-domain multi-physics model are compared in terms of the fundamental frequency and internal forces (shear forces and bending moments). The comparison is carried out both graphically, by presenting envelopes of maximum internal forces along the structure, as well as quantitatively, by calculating the maximum relative difference between the two models. These differences are computed as the value of the variable of interest obtained through the multi-physics model minus that obtained from the simplified one over the reference value of the multi-physics model. Thus, it should be noted that a positive value for the relative difference indicates that the value obtained with OpenFAST is higher than that of the simplified model, while a negative value indicates the opposite.

It is also important to highlight the difference in computational time between the two models. For the simulations conducted in this study, the advanced time-domain multi-physics tool OpenFAST requires approximately 2 h per case, while the simplified static-equivalent model completes each simulation in less than a second.

4.1. Fundamental Frequency Estimation

The analysis of fundamental frequencies constitutes the first step in comparing the two studied models. These frequencies, which are intrinsic characteristics of the system and depend on factors such as stiffness and mass, allow us to determine if the modeled systems are similar.

In the OpenFAST model, the monopile–OWT system’s fundamental frequency is obtained from the fore-aft accelerations at the tower top under parked conditions and without environmental loads. The 400 s of simulation are used to obtain the response for both fixed-base and flexible-base conditions. The Power Spectral Density (PSD) is shown in Figure 2, where the peak values of the fundamental frequencies are indicated

by dashed lines. On the other hand, as described in Section 2.1.1, the simplified model allows for the estimation of the fundamental frequency of the system directly by solving the eigenvalue problem.

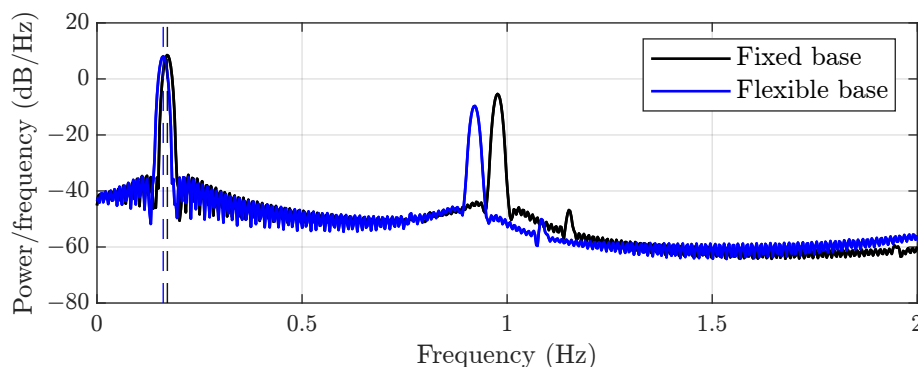


Figure 2. Power Spectral Densities in the fore-aft direction obtained in parked conditions computed using the OpenFAST model.

The analysis of the fundamental frequency reveals that its values are consistent across both models. The fixed-base model shows a fundamental frequency of 0.1724 Hz for the simplified model and 0.1717 Hz for OpenFAST, with a difference of -0.41% . Similarly, the flexible-base model shows a fundamental frequency of 0.1619 Hz for the simplified model and 0.1617 Hz for OpenFAST, with a difference of -0.12% . These minimal differences indicate that both structural models present, at least for their first mode, similar dynamic characteristics. Additionally, these results demonstrate that the SSI effects are equally captured by both models. In the studied problem, the effects of the foundation's flexibility produce a variation of approximately -6% with respect to the fixed-base fundamental frequency, exceeding the 5% safety margin considered by recommended practices [3].

4.2. Wind Load Scenarios

Figure 3 shows the envelopes of maximum shear forces and bending moments for the wind-only scenarios. Results corresponding to different wind velocities (5 m/s, 10 m/s, 15 m/s, 20 m/s, and 25 m/s) are plotted in different colors, while each column presents the results for the different turbulence conditions. The solid lines present the results of the time-domain multi-physics tool OpenFAST, while the dashed lines presents those of the simplified model.

The results show that the maximum internal forces are found when the wind velocity is close to the rated wind velocity (around 10 m/s). The evolution of the shear forces and bending moments along the structure is similar for the three studied turbulence models. However, the influence of the wind velocity is more important for the extreme turbulence model. Comparing the results obtained with the OpenFAST software and the simplified model, similar maximum bending moments are reached through both models for the NTM and ETM turbulence levels. However, larger discrepancies are found for the extreme turbulence conditions. On the other hand, for the shear forces, significant differences are found between the simplified and multi-physics models. It is also important to note that, due to the isostatic behavior of the simplified model, shear forces and bending moments monotonically increase from the rotor to the mudline level. The envelopes of maximum internal forces obtained through OpenFAST show some oscillations that indicate dynamic effects, with the more remarkable difference being the non-zero bending moments at the hub level induced by the inertia or the rotor.

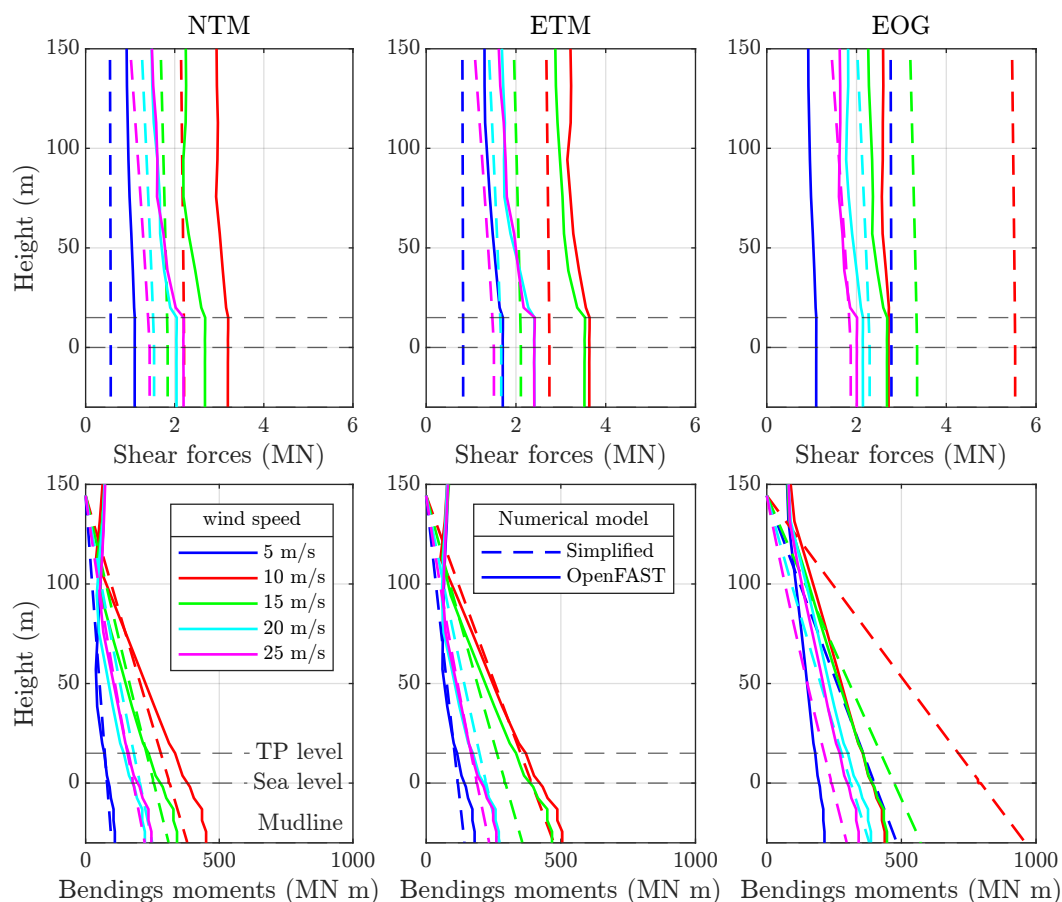


Figure 3. Envelopes of maximum shear forces and bending moments along the structure due to wind-only scenarios.

To better quantify the differences between the two considered structural models, Tables 7 and 8 present, respectively, the maximum shear forces and bending moments for the wind-only scenarios. Only results at the mudline level are included as relevant points of analysis. In each column, the values corresponding to different mean wind velocities are displayed, while the different turbulence models are sorted in groups organized by rows. These results are also presented in Figure 4, which clearly illustrates that turbulence models and wind velocities have a significant impact on the response of OWTs and on the suitability of the simplified static-equivalent model.

Table 7. Maximum shear forces in MN at mudline level due to wind-only scenarios.

Wind Velocity (m/s)		5	10	15	20	25
Normal Turbulence Model (NTM)	Simplified Model	0.56	2.21	1.84	1.54	1.44
	OpenFAST	1.10	3.19	2.68	2.04	2.20
	Difference (%)	48.79	30.77	31.27	24.67	34.65
Extreme Turbulence Model (ETM)	Simplified Model	0.82	2.75	2.11	1.67	1.51
	OpenFAST	1.71	3.63	3.53	2.41	2.41
	Difference (%)	51.75	24.46	40.17	30.66	37.35
Extreme Operating Gust (EOG)	Simplified Model	2.78	5.53	3.35	2.29	1.87
	OpenFAST	0.86	2.30	2.37	2.14	1.85
	Difference (%)	−223.80	−140.91	−41.35	−6.98	−1.08

Table 8. Maximum bending moments in MN m at mudline level due to wind-only scenarios.

Wind velocity (m/s)		5	10	15	20	25
Normal Turbulence Model (NTM)	Simplified Model	97.18	380.74	310.65	249.44	221.45
	OpenFAST	109.36	450.75	341.94	221.68	246.11
	Difference (%)	11.13	15.53	9.15	−12.52	10.02
Extreme Turbulence Model (ETM)	Simplified Model	142.42	474.10	357.38	272.92	234.08
	OpenFAST	179.81	505.19	467.29	269.60	260.58
	Difference (%)	20.79	6.15	23.52	−1.23	10.17
Extreme Operating Gust (EOG)	Simplified Model	483.15	960.42	573.68	381.10	297.16
	OpenFAST	214.26	438.00	446.35	386.78	341.21
	Difference (%)	−125.50	−119.27	−28.53	1.47	12.91

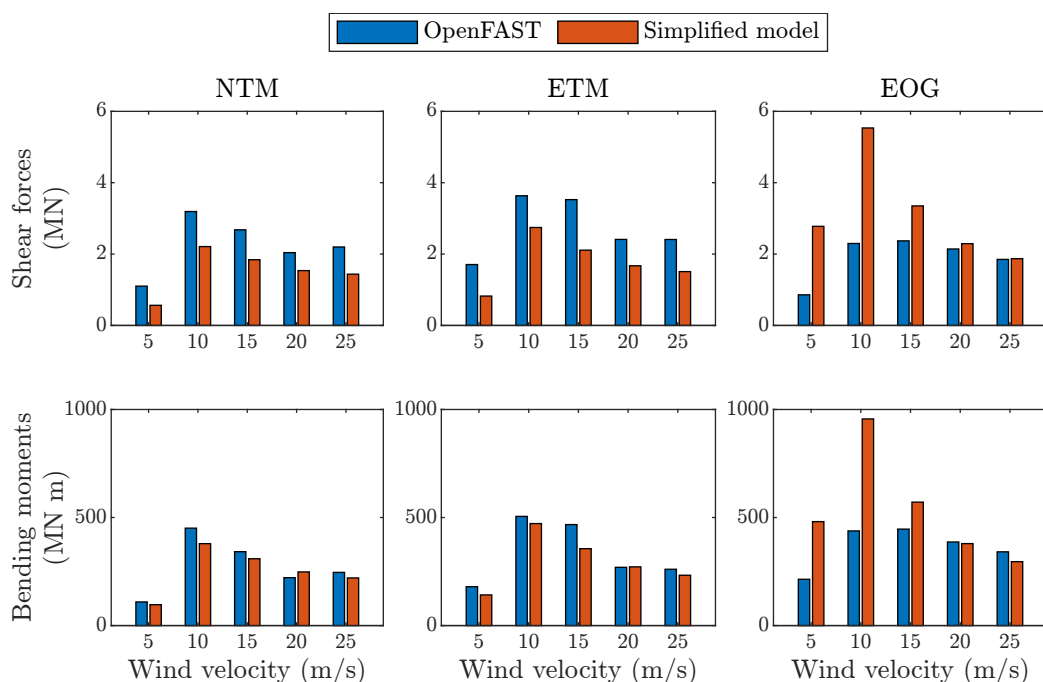


Figure 4. Maximum shear forces and bending moments at mudline level due to wind-only scenarios.

As commented on before, the maximum responses are reached at wind velocities close to the rated wind velocity. This finding is consistent with the results obtained by Arany et al. [6]. On the other hand, turbulence plays a crucial role in influencing shear forces and bending moments. In scenarios with low turbulence, such as the NTM or ETM, both structural models produce similar bending moments, with maximum differences of around 20%. However, assuming high turbulence (EOG) results in a significantly greater response in the simplified static-equivalent model, reaching differences of around −120%. This outcome aligns with the expectation that the EOG assumption, as derived from Arany et al. [6], is an over-conservative estimation of this turbulence. In terms of shear forces, a similar effect is observed, but, in general, larger discrepancies are found: around 50% for moderate-turbulence scenarios and −220% for high-turbulence scenarios.

4.3. Environmental Load Scenarios

The envelopes of maximum shear forces and bending moments obtained for the four environmental load scenarios are presented in Figure 5. Each color corresponds to a different load scenario, while the line type denotes the structural model. The influence of wave loads on the distribution of shear forces can easily be seen by comparing these results with the those for the wind-only loads (Figure 3). Near sea level, the shear forces

rapidly increases with depth due to the action of wave loads. This increment is reduced for points near the mudline level as the wave loads vanish. On the contrary, wind loads mainly govern the bending moments of the structure, which almost linearly increase from the hub height to the seabed. The two structural models present similar distributions of internal forces, but their values differ depending on the case. Again, the largest differences are found for the load case that involves the extreme operating gust at the rated wind velocity (E-3), and the simplified model overestimates the results of OpenFAST, especially in terms of bending moments. For the rest of the environmental load scenarios, a fairly good agreement is found in terms of bending moments.

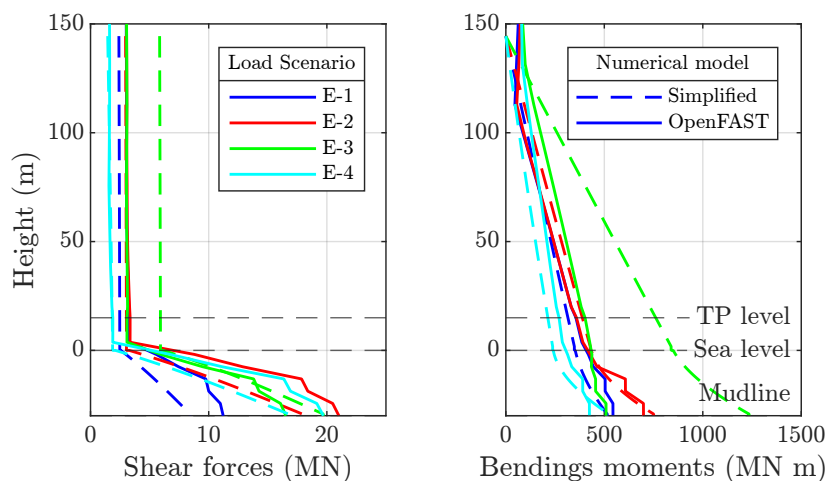


Figure 5. Envelopes of maximum shear forces and bending moments along the structure due to environmental load scenarios.

The maximum shear forces and bending moments at the transition piece and mudline level due to the environmental load scenarios are presented in Tables 9 and 10, respectively, to quantify the relative difference between the two models. Figure 6 also presents these values for a visual comparison. It is clearly seen that the system response in scenario E-3 is substantially higher in the simplified model than in OpenFAST. This overestimation is consistent with the conclusions presented by Jawalageri et al. [16], which is attributed to the conservative approach for the load combination proposed by Arany et al. [6]. Also, another main difference between the two models is the fact that dynamic effects are not considered in the simplified model, apart from for the DAF wave load amplification. Dynamic effects, such as aeroelastic damping, are especially relevant in the E-3 scenario, for which the wind load presents high variability.

Table 9. Maximum shear forces in MN at transition piece and mudline level due to environmental load scenarios.

Environmental Scenarios		E-1	E-2	E-3	E-4
Transition piece	Simplified Model	2.47	3.04	5.92	1.84
	OpenFAST	3.27	3.35	3.09	1.89
	Difference (%)	24.56	9.39	−91.72	2.62
Mudline level	Simplified Model	8.43	17.93	19.70	16.76
	OpenFAST	11.23	21.01	16.53	19.70
	Difference (%)	24.90	14.69	−19.16	14.94

In the context of shear forces at the transition piece and mudline level due to environmental load scenarios, the data reveal a variance between the simplified and OpenFAST models. For instance, at the transition piece level, the simplified model predicts a shear

force of 5.92 MN for scenario E-3, which is a stark contrast to the 3.09 MN predicted by OpenFAST, resulting in a -91.72% difference. Similarly, at the mudline level, the simplified model's prediction of 19.70 MN is higher than OpenFAST's 16.53 MN, with a difference of -19.16% . For the rest of the environmental load scenarios, the simplified model underestimates the shear forces obtained by OpenFAST with a relative difference of around 20% in normal operating conditions (E-1) and up to 15% in the E-2 and E-4 scenarios.

Table 10. Maximum bending moments in MN m at transition piece and mudline level due to environmental load scenarios.

Environmental Scenarios		E-1	E-2	E-3	E-4
Transition piece	Simplified Model	316.63	390.10	764.38	214.29
	OpenFAST	355.90	358.69	402.25	270.06
	Difference (%)	11.04	-8.76	-90.03	20.65
Mudline level	Simplified Model	521.15	763.87	1249.93	535.81
	OpenFAST	543.95	699.00	508.97	424.35
	Difference (%)	4.19	-9.28	-145.58	-26.27

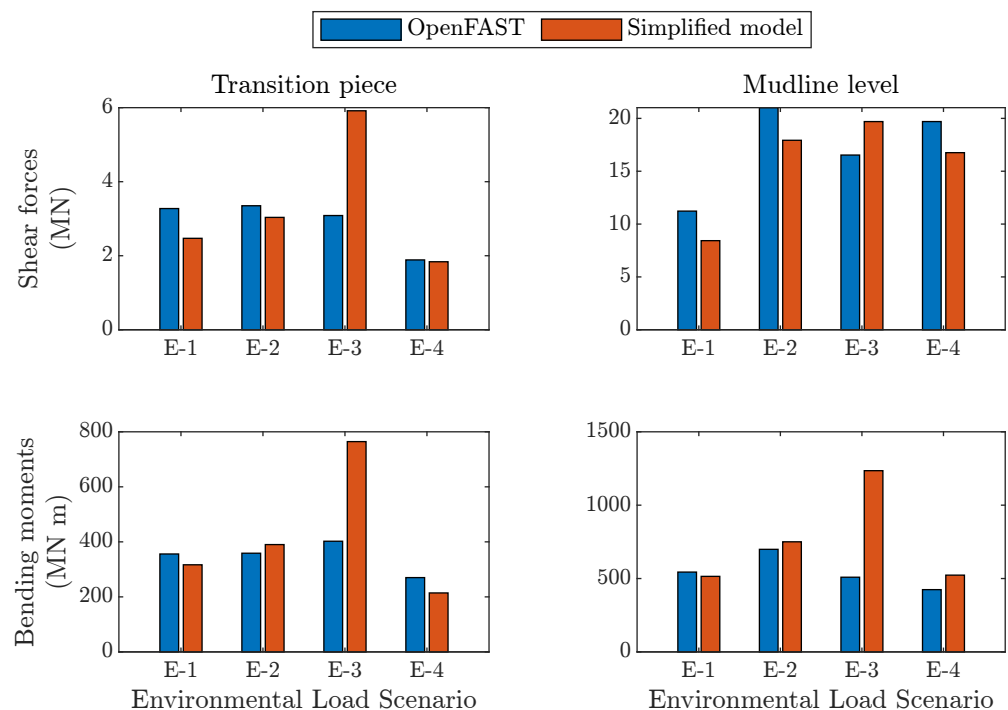


Figure 6. Maximum shear forces and bending moments at transition piece and mudline level due to environmental load scenarios.

Regarding the maximum bending moments at the mudline level due to environmental load scenarios, the simplified model is found to overestimate their values for all scenarios except for normal operating conditions. A good agreement is obtained for the E-1 and E-2 scenarios, with relative differences below 10%, and an acceptable difference is found for the E-4 scenario (25%). However, for the E-3 scenario, the simplified model is extremely conservative, leading to a maximum value that is 145% higher with respect to the OpenFAST simulation.

Analyzing the OpenFAST results, it is found that the E-2 scenario is the most unfavorable one, presenting a maximum shear force of 21 MN and a maximum bending moment of 699 MN at the mudline level. For this load case, the simplified model is able to estimate

these values with differences of around 15% and -9% , respectively. Thus, the use of this model with negligible computational costs for a preliminary design stage is justified.

5. Conclusions

This paper aimed to help elucidate whether or not a simplified static-equivalent model can be used to predict major trends in the dynamic structural response of monopile OWTs. To do so, this study presents a comparison between the results of two numerical models of different levels of complexity used to estimate the structural response of an OWT under dynamic loads: an advanced time-domain multi-physics tool, namely OpenFAST, and a simplified static-equivalent model. For this purpose, the manuscript presented a comparison between the results obtained from both models for the dynamic structural response of the IEA-15-240-RWT reference wind turbine [37], including soil–structure interaction effects. More precisely, the two structural models were compared in terms of their fundamental frequencies and through the analysis of shear forces and bending moments under wind-only and combined wave and wind load scenarios.

The comparison between the fundamental frequencies yielded by both models showed that the simplified lumped model can effectively represent the system's mass and stiffness characteristics. Furthermore, the reduction in the fundamental frequency derived from the SSI effects is practically the same for the two models.

Regarding the wind-only load response, the results showed that turbulence and wind velocity have a significant impact on shear forces and bending moments. Wind velocities near the rated wind speed generated the highest internal forces, particularly at the mudline level. The ability of the simplified model to reproduce the OpenFAST results is directly related to the turbulence level, presenting a better agreement for low-turbulence scenarios. Also, significantly larger discrepancies between the models were found for shear forces compared to bending moments.

For the relevant environmental load scenarios considered, similar conclusions were obtained. In general, the simplified model underestimates the shear forces at the mudline level for low-turbulence scenarios, with 25% relative differences, and it overestimates them for high-turbulence scenarios, reaching over 20% relative differences. On the other hand, the bending moments at the mudline level are generally overestimated by the simplified model, reaching relative differences of around 20% or 125% for low- and high-turbulence scenarios. Considering OpenFAST's results, the maximum internal forces were obtained for the E-2 scenario (ETM and EWH-50 yr). For this worst-case scenario, the simplified model was able to estimate the maximum shear forces and bending moments with relative differences of below 15% and 10%, respectively.

This study reveals that, as expected, the simplified static-equivalent model does not offer sufficient accuracy for its use in final design stages or for the study of specific load scenarios involving high turbulence. However, its conservative nature, limited errors in relevant scenarios, and practically negligible computational costs make this simplified model a viable and interesting option in preliminary analyses, parametric analyses, and the initial stages of the design process, where a high number of evaluations are needed and a high level of accuracy in each simulation is not yet required. For the same reasons, this model could also be suitable for the generation of large datasets developed to train Machine Learning models.

Supplementary Materials: The code of the simplified model can be downloaded at <https://www.mdpi.com/article/10.3390/app15031633/s1>.

Author Contributions: Conceptualization, A.J.R.-M., C.R.-S., G.M.Á. and L.A.P.; methodology, A.J.R.-M. and G.M.Á.; software, A.J.R.-M. and C.R.-S.; validation, A.J.R.-M. and C.R.-S.; formal analysis, A.J.R.-M.; investigation, A.J.R.-M.; data curation, A.J.R.-M.; writing—original draft preparation, A.J.R.-M.; writing—review and editing, C.R.-S., G.M.Á. and L.A.P.; visualization, A.J.R.-M.; supervision, C.R.-S. and G.M.Á.; project administration, L.A.P.; funding acquisition, L.A.P. All authors have read and agreed to the published version of the manuscript.

Funding: This research was funded by the Agencia Estatal de Investigación of Spain (MCIN/AEI/10.13039/501100011033) through research project PID2020-120102RB-I00. In addition, A.J. Romero-Monzón is a recipient of a collaboration grant (23CO1/006519) from the Ministerio de Educación y Formación Profesional, and C. Romero-Sánchez is a recipient of a research fellowship (TESIS2022010011) from the Program of predoctoral fellowships from the Consejería de Economía, Conocimiento y Empleo (Agencia Canaria de la Investigación, Innovación y Sociedad de la Información) of the Gobierno de Canarias and Fondo Social Europeo.

Data Availability Statement: The raw data supporting the conclusions of this article will be made available by the authors on request.

Conflicts of Interest: The authors declare no conflicts of interest.

Abbreviations

The following abbreviations are used in this manuscript:

OWT	Offshore Wind Turbine
SSI	Soil–Structure Interaction
NREL	National Renewable Energy Laboratory
IEC	International Electrotechnical Commission
DNV	Det Norske Veritas
NTM	Normal Turbulence Model
ETM	Extreme Turbulence Model
EOG	Extreme Operating Gust
ESS	Extreme Sea State
EPH	Extreme Wave Height
DAF	Dynamic Amplification Factor
LPM	Lumped Parameter Model
PSD	Power Spectral Density
TP	Transition Piece

References

1. Global Wind Energy Council. *Global Offshore Wind Report 2024*; Technical Report; GWEC: Brussels, Belgium, 2024.
2. IEC 61400-1:2020; Wind Energy Generation Systems—Part 1: Design Requirements. International Electrotechnical Commission: Geneva, Switzerland, 2020.
3. Det Norske Veritas. *DNV-GL-ST-0126: Support Structures for Wind Turbines*; Det Norske Veritas: Bærum, Norway, 2016.
4. Det Norske Veritas. *DNV-GL-ST-0437: Loads and Site Conditions for Wind Turbines*; Det Norske Veritas: Bærum, Norway, 2016.
5. McCoy, A.; Musial, W.; Hammond, R.; Mulas Hernandez, D.; Duffy, P.; Beiter, P.; Perez, P.; Baranowski, R.; Reber, G.; Spitsen, P. *Offshore Wind Market Report: 2024 Edition*; Technical Report; National Renewable Energy Laboratory (NREL): Golden, CO, USA, 2024.
6. Arany, L.; Bhattacharya, S.; Macdonald, J.; Hogan, S.J. Design of monopiles for offshore wind turbines in 10 steps. *Soil Dyn. Earthq. Eng.* **2017**, *92*, 126–152. [[CrossRef](#)]
7. Luo, R.; Wang, A.; Li, J.; Ding, W.; Zhu, B. Simplified Design Method of Laterally Loaded Rigid Monopiles in Cohesionless Soil. *J. Mar. Sci. Eng.* **2024**, *12*, 208. [[CrossRef](#)]
8. Burd, H.J.; Taborada, D.M.; Zdravković, L.; Abadie, C.N.; Byrne, B.W.; Houlby, G.T.; Gavin, K.G.; Igoe, D.J.; Jardine, R.J.; Martin, C.M.; et al. PISA design model for monopiles for offshore wind turbines: Application to a marine sand. *Géotechnique* **2020**, *70*, 1048–1066. [[CrossRef](#)]
9. Mendoza, A.S.E.; Griffith, D.T.; Qin, C.; Loth, E.; Johnson, N. Rapid approach for structural design of the tower and monopile for a series of 25 MW offshore turbines. *J. Phys. Conf. Ser.* **2022**, *2265*, 032030. [[CrossRef](#)]

10. Burd, H.J.; Abadie, C.N.; Byrne, B.W.; Houlsby, G.T.; Martin, C.M.; McAdam, R.A.; Jardine, R.J.; Pedro, A.M.; Potts, D.M.; Taborda, D.M.; et al. Application of the PISA design model to monopiles embedded in layered soils. *Géotechnique* **2020**, *70*, 1067–1082. [[CrossRef](#)]
11. Jonkman, J. *Definition of a 5-MW Reference Wind Turbine for Offshore System Development*; National Renewable Energy Laboratory Technical Report; National Renewable Energy Laboratory: Golden, CO, USA, 2009.
12. Luan, Z.; Dou, P.; Chen, Y.; Zhang, H.; Ku, Y. Optimization Study of a Tuned Mass Damper for a Large Monopile Wind Turbine. *Energies* **2024**, *17*, 4460. [[CrossRef](#)]
13. Jonkman, J. *FAST User's Guide*; National Renewable Energy Laboratory Technical Report; National Renewable Energy Laboratory: Golden, CO, USA, 2005.
14. Barahona, B.; Jonkman, J.M.; Damiani, R.; Robertson, A.; Hayman, G. Verification of the new FAST v8 capabilities for the modeling of fixed-bottom offshore wind turbines. In Proceedings of the 33rd Wind Energy Symposium, Kissimmee, FL, USA, 5–9 January 2015; p. 1205.
15. Jonkman, J.M. Dynamics of offshore floating wind turbines—model development and verification. *Wind. Energy Int. J. Prog. Appl. Wind. Power Convers. Technol.* **2009**, *12*, 459–492. [[CrossRef](#)]
16. Jawalageri, S.; Bhattacharya, S.; Jalilvand, S.; Malekjafarian, A. A comparative study on load assessment methods for offshore wind turbines using a simplified method and OpenFAST simulations. *Energies* **2024**, *17*, 2189. [[CrossRef](#)]
17. Rodríguez-Galván, E.; Álamo, G.M.; Medina, C.; Maeso, O. Influence of seabed profile on the seismic response of monopile-supported offshore wind turbines including dynamic soil-structure interaction. *Mar. Struct.* **2023**, *92*, 103500. [[CrossRef](#)]
18. Álamo, G.M.; Martínez-Castro, A.E.; Padrón, L.A.; Aznárez, J.J.; Gallego, R.; Maeso, O. Efficient numerical model for the computation of impedance functions of inclined pile groups in layered soils. *Eng. Struct.* **2016**, *126*, 379–390. [[CrossRef](#)]
19. Álamo, G.M.; Bordón, J.D.; Aznárez, J.J. On the application of the beam model for linear dynamic analysis of pile and suction caisson foundations for offshore wind turbines. *Comput. Geotech.* **2021**, *134*, 104107. [[CrossRef](#)]
20. Chandrasekaran, S. *Dynamic Analysis and Design of Offshore Structures*; Springer: Singapore, 2015; Volume 761.
21. Liang, F.; Yuan, Z.; Liang, X.; Zhang, H. Seismic response of monopile-supported offshore wind turbines under combined wind, wave and hydrodynamic loads at scoured sites. *Comput. Geotech.* **2022**, *144*, 104640. [[CrossRef](#)]
22. Wang, P.; Zhao, M.; Du, X.; Liu, J.; Xu, C. Wind, wave and earthquake responses of offshore wind turbine on monopile foundation in clay. *Soil Dyn. Earthq. Eng.* **2018**, *113*, 47–57. [[CrossRef](#)]
23. Det Norske Veritas. *DNV-RP-C205: Environmental Conditions and Environmental Loads*; Det Norske Veritas: Bærum, Norway, 2010.
24. National Renewable Energy Laboratory. OpenFAST Documentation. Release v4.0.0. 2024. Available online: <https://openfast.readthedocs.io/en/main/> (accessed on 10 February 2024).
25. Jonkman, J.M.; Hayman, G.; Jonkman, B.; Damiani, R.; Murray, R. *AeroDyn v15 User's Guide and Theory Manual*; NREL Draft Report; National Renewable Energy Laboratory (NREL): Golden, CO, USA, 2015; Volume 46.
26. National Renewable Energy Laboratory. TurbSim. Available online: <https://www.nrel.gov/wind/nwtc/turbsim.html> (accessed on 2 April 2024).
27. Platt, A.; Jonkman, B.; Jonkman, J. *InflowWind User's Guide*; NREL Technical Report; National Renewable Energy Laboratory (NREL): Golden, CO, USA, 2016.
28. OpenFast. ElastoDyn Users Guide and Theory Manual. Available online: <https://kitefast.readthedocs.io/en/kitefast/source/user/elastodyn/> (accessed on 12 April 2024).
29. Jonkman, J.M.; Robertson, A.; Hayman, G.J. *HydroDyn User's Guide and Theory Manual*; National Renewable Energy Laboratory: Golden, CO, USA, 2014.
30. Damiani, R.; Jonkman, J.; Hayman, G. *SubDyn User's Guide and Theory Manual*; Technical Report; National Renewable Energy Laboratory (NREL): Golden, CO, USA, 2015.
31. Romero-Sánchez, C.; Padrón, L.A. An implementation of multi-support input motion into openfast for the earthquake analysis of offshore wind turbines. In Proceedings of the 9th International Conference on Computational Methods in Structural Dynamics and Earthquake Engineering (COMPdyn 2023), Athens, Greece, 12–14 June 2023.
32. Romero-Sánchez, C.; Padrón, L.A. Influence of wind and seismic ground motion directionality on the dynamic response of four-legged jacket-supported Offshore Wind Turbines. *Eng. Struct.* **2024**, *300*, 117191. [[CrossRef](#)]
33. Carbonari, S.; Morici, M.; Dezi, F.; Leoni, G. A lumped parameter model for time-domain inertial soil-structure interaction analysis of structures on pile foundations. *Earthq. Eng. Struct. Dyn.* **2018**, *47*, 2147–2171. [[CrossRef](#)]
34. González, F.; Padrón, L.A.; Carbonari, S.; Morici, M.; Aznárez, J.J.; Dezi, F.; Leoni, G. Seismic response of bridge piers on pile groups for different soil damping models and lumped parameter representations of the foundation. *Earthq. Eng. Struct. Dyn.* **2019**, *48*, 306–327. [[CrossRef](#)]
35. Morici, M.; Minnucci, L.; Carbonari, S.; Dezi, F.; Leoni, G. Simple formulas for estimating a lumped parameter model to reproduce impedances of end-bearing pile foundations. *Soil Dyn. Earthq. Eng.* **2019**, *121*, 341–355. [[CrossRef](#)]

36. Padrón, L.A.; Carbonari, S.; Dezi, F.; Morici, M.; Bordón, J.D.; Leoni, G. Seismic response of large offshore wind turbines on monopile foundations including dynamic soil–structure interaction. *Ocean. Eng.* **2022**, *257*, 111653. [[CrossRef](#)]
37. Gaertner, E.; Rinker, J.; Sethuraman, L.; Zahle, F.; Anderson, B.; Barter, G.; Abbas, N.; Meng, F.; Bortolotti, P.; Skrzypinski, W.; et al. *Definition of the IEA 15-Megawatt Offshore Reference Wind Turbine*; National Renewable Energy Laboratory: Golden, CO, USA, 2020.

Disclaimer/Publisher’s Note: The statements, opinions and data contained in all publications are solely those of the individual author(s) and contributor(s) and not of MDPI and/or the editor(s). MDPI and/or the editor(s) disclaim responsibility for any injury to people or property resulting from any ideas, methods, instructions or products referred to in the content.